Large, Negative Magnetoresistance in an Oleic Acid-Coated Fe_3O_4 Nanocrystal Self-assembled Film

Shigemi Kohiki, Tomoki Kinoshita, Koichiro Nara, Kotone Akiyama-Hasegawa*[§]*, and Masanori Mitome*[§]

Department of Materials Science, Kyushu Institute of Technology, 1-1 Sensui, Tobata, Kitakyushu 804-8550, Japan

[§]International Center for Materials Nanoarchitectonics, National Institute for Materials Science, 1-1 Namiki, Tsukuba, Ibaraki 305-0044, Japan

*To whom correspondence should be addressed: kohiki@che.kyutech.ac.jp

ABSTRACT An oleic acid-coated Fe_3O_4 nanocrystal self-assembled film was fabricated via drop casting of colloidal particles on a SiO_2/Si substrate. The film exhibited bifurcation of the zero-field-cooled and field-cooled magnetizations around 250K. The nonlinear current-voltage (*I-V*) characteristics between the source and drain electrodes in both zero and non-zero magnetic fields (*H*) were observed above and below the bifurcation temperature. A large negative magnetoresistance (MR ≈ −60%) was achieved at 200K and *H* = 1 T. Even at 295K and 0.2 T,

the negative MR (≈ −50%) persisted. A Fowler-Nordheim plot and power-law scaling of the *I-V* characteristics revealed that the current flows through two-dimensional (2D) percolated electron tunneling paths. The enlargement of MR can be attributed to spin-dependent electron tunneling between magnetically coupled Fe_3O_4 nanocrystals self-assembled in 2D ordered arrays.

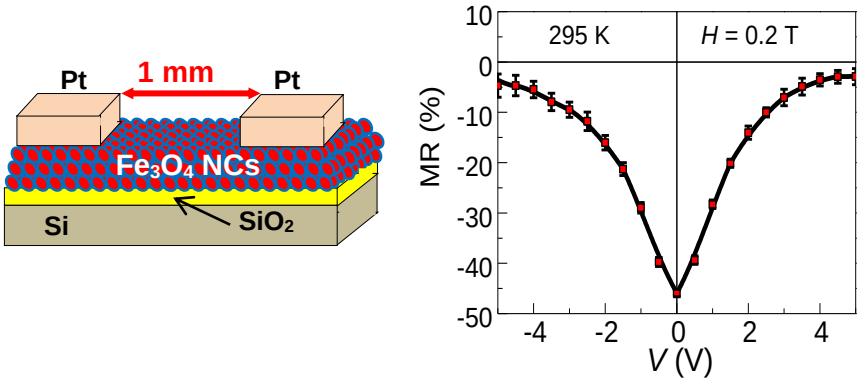

KEYWORDS Negative Magnetoresistance, Fe_3O_4 Nanocrystals, Oleic Acid, Self-assembly, Two-dimensional Networks

INTRODUCTION

Magnetoresistance (MR) in half-metals has been the focus of basic and applied studies for spintronics device applications. Half-metals are conductors with a continuous energy band at the Fermi level for one spin channel, and insulators with an energy gap at the Fermi level for another spin channel. The half-metal Fe_3O_4 is suitable for spintronic devices operating above room temperature (RT) because it has fully spin-polarized (P = 100%) carriers up to its Curie temperature (≈ 840K) [1,2]. Thus, it should be possible to employ the large, negative MR of an oleic acid (OA)-coated Fe_3O_4 nanocrystal (NC) self-assembled film [3] to switch the current

between the source and drain electrodes of a two-terminal spin device, and the large MR should bring about very high performance.

In multiple junction systems consisting of Fe_3O_4 NCs weakly electrically contacting one another via thin, insulating OA barriers, the MR is defined as MR = $(R_H - R_0)/R_0$, where R_H and R_0 are the differential resistance ($R = dV/dI$) for nonlinear source-drain current and bias-voltage (I-V) characteristics in non-zero ($H \neq 0$) and zero ($H = 0$) magnetic fields, respectively. Each Fe_3O_4 NC possesses spontaneous magnetization along the [111] easy axis. When the angle between the magnetization of adjacent Fe_3O_4 NCs in three-dimensional (3D) systems is denoted by θ, the relative magnetization of the system m relates to θ as $m^2 = \langle\cos\theta\rangle$ [4]. Application of a sufficiently strong field ($H \neq 0$) entirely changes the configuration of magnetizations in the system to be in parallel (θ = 0), and then maximizes the spin-dependent electron tunneling probability between the NCs by fulfilling the condition $m = 1$. When the tunneling resistivity is varied from high to low, the sign of MR becomes negative [5]. Since MR is connected to P and m by MR ≡ $P^2m^2/(1 + P^2m^2)$ [4], then both P = 100% and $m = 1$ are required to maximize MR (= −50%) in 3D systems.

Even at RT, P = 100% is theoretically expected for Fe_3O_4. Poddar et al. reported an MR of −300% at 110K and −125% above 150K in 0.25 T for OA-encapsulated Fe_3O_4 nanoparticles [6]. Zeng et al. reported an MR = −35% at 60K in 3.5 T for organic surfactant-covered Fe_3O_4 nanoparticles with a superparamagnetic blocking temperature (T_b) of 40K [7]. Wang et al. reported an MR = −40.9% at 110K in 14 T for a 3D network of spherical Fe_3O_4 particles dispersed in polystyrene [8]. Wang et al. reported an MR = −10.8% at 1 T and −17% at 8 T for SiO_2-coated nanospheres of Fe_3O_4 [9]. Kant et al. reported an MR at 100K of −11.5% and −5.8% in 1 T for Fe_3O_4 nanoparticles coated with thin SiO_2 and ZnO layers, respectively [10]. They

reported a T_b = 200K for the samples. Wang et al. [11] reported an MR in 5 T of −21% at 130K and −13% at 280K for Fe_3O_4 nanoparticles dispersed in hexabromobenzene. Wang et al. [12] reported an MR in 0.58 T of −17% at 115K and −7% at RT for OA-covered Fe_3O_4 nanoparticles. They also reported that an inter-particle separation (s) of ≈4 nm by surface-coated OA molecules enhanced the MR by more than two times over uncoated Fe_3O_4 nanoparticles. The rather large MR values below 130K for the Fe_3O_4 nanoparticle systems reflect an increase in the resistivity due to the Verwey transition in the Fe_3O_4 crystal lattice [13]. Taub et al. reported an MR of –25% at 250K in 0.8 T for OA-coated Fe_3O_4 nanoparticles with a T_b of ~220K [14]. They also reported the temperature dependence of MR exhibiting a maximum around T_b. However, the value of MR, even at T_b, was far from −50%. As mentioned above, the rather large MR values for superparamagnetic 3D systems reflect the intra-particle Verwey transition.

Previously, we reported that two-dimensional (2D) hexagonal networks of OA-$Fe_{2.5}Mn_{0.5}O_4$ NCs exhibit both a spin glass (SG) transition around 150K and a large MR ≈ −40% at 200K in H = 0.5 T [3]. Enlargement of MR can be achieved by building 2D ordered arrays of the NCs, in which geometrically frustrated networks of collinear magnetic moments increase R_0 and decease R_H in intergranular tunneling of spin-polarized electrons. The spontaneous self-assembly phenomenon is commonly used to control the arrangement of the NCs into hexagonally ordered arrays [15,16]. Oleic acid, $CH_3(CH_2)_7CH=CH(CH_2)_7COOH$, is an unsaturated carboxylic acid with a *cis*-double-bond "kink" in the middle of its C_{18} tail. The polar head group chemisorbs to the hydrophilic surface of nanoparticles, and steric repulsion of the long chain prevents the NCs from agglomerating [17]. Since OA-NCs are hydrophobic, the slow drying of a hexane colloidal suspension dropped onto a substrate results in a self-assembled film with hexagonally-aligned

NC arrays. Furthermore, hydrophobization by OA is highly advantageous in preventing the lowering of observed spin-polarization due to surface oxidation of Fe_3O_4 NCs [18].

As a foundation for a high-performance spin device, the MR of a drop-cast OA-Fe_3O_4 NC self-assembled film was examined. Nonlinear *I-V* characteristics were observed above 200K in $H < 1$ T. At 200 K, the MR of the film reached −54% at 0.5 T and −58% at 1 T. Even at 295K, the MR value of the film remained at −46% in 0.2 T. The observed MR values at 200K are larger than the maximum possible (−50%) for 3D systems with $P = 100\%$ and $m = 1$. A Fowler-Nordheim plot and power-law scaling of the *I-V* curves clarified that the current flows through 2D percolated electron tunneling paths formed in the film. The MR larger than −50% was achieved by spin-dependent electron tunneling between magnetically-coupled Fe_3O_4 nanocrystals self-assembled in 2D ordered arrays.

EXPERIMENTAL

Synthesis of Fe_3O_4 NCs and Fabrication of the NC Self-assembled Film. Fe_3O_4 NCs were synthesized from $Fe(acac)_3$ in a solution of dibenzylether mixed with OA [21]. $Fe(acac)_3$, dibenzylether, and OA, in a molar ratio of 6 : 157 : 12, were mixed with vigorous stirring for an hour at RT, and then the mixture was refluxed at 573 K for half an hour. After cooling to RT, the NCs were precipitated from the crude solution by adding a mixture of toluene:hexane (1:1) followed by centrifugation. The precipitated NCs were washed with anhydrous chloroform. The Fe_3O_4 NCs were dispersed in a weak alkaline (pH = 10.4) aqueous solution. After stirring for 10 minutes, additional OA (molar ratio of [Fe] : $[C_{18}H_{34}O_2]$ = 1 : 42) was added to the solution with vigorous stirring. After stirring for 20 minutes, 1N HCl aqueous solution was added to neutralize the solution. After removal of the transparent solvent, the precipitated OA-Fe_3O_4 NCs were

dispersed in hexane. The OA-Fe_3O_4 NCs were used without post-preparative size selection for fabrication of the self-assembled film. The colloidal suspensions in hexane were dropped onto a SiO_2/Si substrate, and then dried at 573 K for half an hour at 100 Pa to yield the OA-Fe_3O_4 NC self-assembled film.

Structural, Magnetic and Magnetoelectric Characterization. The crystal structures of the NCs and the NC self-assembled film were confirmed via X-ray diffraction (XRD) using a Rigaku CN2013 X-ray diffractometer with Cu *K*α radiation. The size and shape of the NCs were examined using a JEOL JEM-3100FEF transmission electron microscope (TEM) operated at an electron acceleration voltage of 300 kV.

Magnetic and magnetoelectric characterization was carried out using a superconducting quantum interference device (SQUID) magnetometer (Quantum Design, MPMS-5S). For the temperature dependence of the DC magnetization (*M*-*T*) measurements, the sample was cooled from RT to 5 K in $H = 0$, and then $H = 0.03$ T was applied. The zero-field-cooled (ZFC) magnetization was recorded with rising temperature to 300 K. After the ZFC measurement, the sample was again cooled to 5 K in $H = 0.03$ T, and then the field-cooled (FC) magnetization was recorded with rising temperature to 300 K. Both the real (χ') and imaginary (χ'') parts of the complex susceptibility were measured from 5 to 300 K upon warming in an AC field (H_{AC}) of 3.8 G at a frequency (*f*) of 1-100 Hz. For the magnetoelectric measurements, Pt electrodes were bonded via gold wires to the MPMS-5S system. *H* was applied parallel to *I* between the source and drain electrodes spaced 1 mm apart. For each *I*-*V* measurement, the $H = 0$ character was measured first, followed by the $H \neq 0$.

RESULTS AND DISCUSSION

The as-synthesized NCs demonstrate an XRD pattern attributable to the cubic Fe_3O_4 crystal lattice (a = 0.84 nm) with space group $Fd\bar{3}m$ (JCPDS 19-0629), as shown in Figure 1(a). The crystallite size, estimated from the half-width of the (511) reflection peak using Scherer's equation, amounts to ≈50 nm. The XRD patterns shown in Figure 1(b) indicate that the sample consists of Fe_3O_4 NCs and a SiO_2/Si substrate.

As shown in the upper panel of Figure 2, ordered arrays of NCs having a lateral size (d) of ≈50 nm were built in the self-assembled film. Rows of NCs appear in the film, accompanied with disorder as reported in Ref. [22], and demonstrated a preferred orientation to some extent, as shown in the lower panel of Figure 2. In a 300 × 300 nm^2 region, 36 NCs were typically counted, so the mean area occupied by a single NC (A_{NC}) amounts to 2500 nm^2. Assuming a hexagonal arrangement of the NCs [3], the equation $A_{NC} = (\sqrt{3}/2)(d+s)^2$ gives an s of ≈3 nm, which is in good agreement with that reported in Ref. [23]. The upper panel of Figure 3 shows that the entire NC is a single crystal without stacking faults or twins. The distinctive spots of a nano beam diffraction pattern (Figure 3, lower left panel) from the NC can be simulated well by a centrosymmetric Fe_3O_4 crystal lattice (JCPDS 19-0629) with the incident beam direction along the [110] axis, as shown in the lower right panel. Thus, the Fe_3O_4 NCs composing the self-assembled film are single crystals.

In the field-dependent magnetization (M-H) at 200K, the NCs exhibited a nearly-saturated sigmoidal curve above H ≈0.5 T with M = 1.3 μ_B/Fe, which is equivalent to the spontaneous magnetization of Fe_3O_4. However, the sample possessed a nearly-saturated M of 0.5 μ_B/Fe above H ≈0.2 T, as shown in Figure 4(a). Consequently, the mass percentage of Fe_3O_4 in the sample amounts to approximately 39%.

As shown in Figure 4(b), the sample demonstrated bifurcation of the FC and ZFC magnetizations below 250K. The FC magnetization remained almost constant below 250K, whereas the ZFC fell off gradually with decreasing temperature. Such a cooling history-dependence of the DC magnetization suggests an SG transition around 250K for the sample. With regard to the χ'-T and χ''-T AC characteristics of the ZFC sample, χ' decreased almost linearly with decreasing temperature from 288K to 30K (not shown), while χ'' showed a broad peak around 270K and a narrow peak around 20K, as shown in Figure 4(c). The χ'' anomaly at 20K is an indication of the superspinglass transition in each isolated Fe_3O_4 NC [24], while the one at 270K (the freezing temperature, T_f) peculiar to the film is indicative of the slow dynamics common in self-assembled OA-Fe_3O_4 NCs [25,26]. Such a high T_f reflects the strong dipolar interactions among the magnetic moments of the Fe_3O_4 NCs isolated (≈3 nm apart) by OA molecules adsorbed on their surfaces, and affects the MR, even at RT Below T_f, the sample is in a frustrated magnetic state. With increasing temperature, the frozen magnetic moments thaw progressively. Even at RT, near T_f, the magnetic moments are still frozen partly, switching randomly. The randomly-oriented magnetic moments of the NCs in percolating current paths give rise to an enlarged R_0. An applied field ($H \neq 0$) rotates the magnetic moments of the NCs to mutual alignment (m = 1), and enlarges the spin-polarized tunneling rate for multiple inter-particle junctions, which then results in a largely enhanced negative MR for the sample.

At 200K, the sample demonstrated the nonlinear I-V characteristics typical of an intergranular tunneling conductance mechanism [27], as shown in Figure 5(a). R (= dV/dI) in H = 0 and $H \neq 0$ were high and low, respectively, as seen in Figure 5(b). An applied field (H = 0.5 T) aligned the magnetic moments of the Fe_3O_4 NCs parallel to each other, and enlarged the electron tunneling probability between the spin-polarized conduction bands of adjacent Fe_3O_4 NCs. The dV/dI

curves peaked around $V = 0$ and fell off rapidly with increasing V. The (dV/dI)-V characteristic of a single inter-particle tunneling junction is assumed to be proportional to the density of occupied states of the Fe_3O_4 NC on the source-electrode side, and that of empty states on the drain-electrode side. Electron tunneling at different V probes different energy ranges of the density of states above the Fermi level of the Fe_3O_4 NC on the drain-electrode side. Therefore, the ≈1 V width of the dV/dI peak may be the result of the conduction band of the Fe_3O_4 NCs with a width of ≈0.5 eV. At 200K, an MR of −54% was observed in 0.5 T, and −58% in 1 T. Such a saturation in MR above $H = 0.5$ T is consistent with that in M above $H \approx 0.2$ T. The observed MR below T_f is larger than the value of −50% expected for a 3D Fe_3O_4 NC system with $P = 100\%$ and $m = 1$ [4], however an MR ≈ −120% at 200K in 0.25 T was reported by Poddar et al. [6] for arrays of OA-Fe_3O_4 NCs.

As shown in Figure 6(a), the I-V characteristics of the sample were also measured at 295K under an H perpendicular to I. It is well known that there is no geometrical effect on MR for granular systems. Tripathy et al. [28] reported that, for an Fe_3O_4-Al_2O_3 granular system, the MR measured with H perpendicular to I was identical to that measured with H parallel to I. An anisotropic effect is absent in the MR of granular systems. Even at 295K, the nonlinearity in the I-V characteristics was preserved. As shown in Figure 6(b), the larger dV/dI in 0 T compared to than that in 0.2 T resulted in a negative MR of −46%. Increasing the temperature should lessen the degree of spin polarization near the Fermi level, although a large negative MR was still retained at RT. Assuming $m = 1$, even in $H = 0.2$ T, the MR = −46% corresponds to $P = 93\%$ at RT, which seems to be consistent with the half-metallic nature of Fe_3O_4.

An intergranular tunneling conductance mechanism for the MR of the sample above 150K is supported by the linear relationship in the ln R_0 (= $dV_{|V=0}/dI$) versus $T^{-1/2}$ plot shown in Figure

7(a). Such a $T^{-1/2}$ dependence denotes that the MR of the sample is dominated by direct electron tunneling between adjacent Fe_3O_4 NCs in current paths. A Fowler-Nordheim plot of the *I-V* curves at 200K and 295K, derived from the $V = 0$ limit equation $\ln(I/V^2) \propto \ln(1/V) - [2s(2m_e)^{1/2}/\hbar]\Phi^{1/2}$, where s is the barrier thickness, m_e is the effective mass of the electron, and Φ is the barrier height for electron tunneling [29], are shown in Figures 7(b) and 7(c), respectively. While the plot at 200K demonstrates an inflection point at ≈1.3 V corresponding to a transition from direct tunneling to Fowler-Nordheim tunneling, the plot at 295K shows only logarithmic growth toward the zero *V* limit. The plot sustains the thesis that even at RT, the observed MR is dominated by direct electron tunneling across the OA layer between two adjacent Fe_3O_4 NCs.

The observed nonlinear *I-V* characteristics suggest that the sample is highly insulating below $|V| = 0.5$ V since the tunnel current is blocked due to local charging of the NCs by a single electron. Above the Coulomb blockade threshold ($V_T = 0.5$ V), electron tunneling paths between the source and drain electrodes are opened, and the tunnel current starts to flow via the NCs, not via thermally-activated electron hopping, even at RT, as mentioned above. Since the observed MR (over −50%) cannot be predicted by 3D NC systems [4], the dimensionality of the spin-dependent electron tunneling paths was examined via power-law scaling with the equation $I \sim (V - V_T)^{\xi}$ [19] based on a Coulomb blockade model [20]. The experimental *I-V* characteristics beyond V_T were fitted well with the critical exponents $\xi \approx 1.6$~1.7, as shown in Figure 8. The critical exponents ξ for 1D and 2D NC arrays have been analytically determined to be 1 and 5/3, respectively [20]. There is excellent agreement of the experimental *I-V* characteristics with the scaling law (universal ξ of 5/3), meaning 2D percolated electron tunneling paths are opened above V_T. V_T is amplified by over tenfold in 2D NC arrays due to single electrons charging at multiple sites in the percolation path [20]. It has been reported that below V_T, sequential

tunneling is superseded by coherent tunneling, which is sensitive to the relative orientation of magnetization between the NCs [30]. The Coulomb blockade MR is theoretically expected to reach over 1000% at RT when adjacent NCs couple magnetically [31]. The present MR (≈ −60%) at 200K in 1 T around $V \approx 0$ V is due to spin-dependent electron tunneling between magnetically coupled OA-Fe_3O_4 NCs in self-assembled 2D arrays.

CONCLUSION

A large, negative MR brings about high performance in a normally OFF-type spin-dependent current switch. In an OA-Fe_3O_4 NC self-assembled film exhibiting an SG transition with $T_f \approx$ 270K, nonlinear *I-V* characteristics were observed, resulting in an MR = −54% in 0.5 T and −58% in 1 T at 200K, and −46% in 0.2 T at 295 K. A spin-polarized current flowed through 2D percolated electron tunneling paths. The MR observed is larger than the maximum for 3D systems with both P = 100% and m = 1, and is attributed to an enlarged probability of spin-dependent electron tunneling in the Coulomb blockade region between magnetically coupled Fe_3O_4 NCs self-assembled in 2D ordered arrays.

Acknowledgments. S. K thanks the support of a Yoshida Research Grant for this work. This work was partly supported by the "Nanotechnology Platform Project" of the Ministry of Education, Culture, Sports, Science and Technology, Japan.

Figure 1. XRD pattern of as-synthesized NCs with peaks from the JCPDS 19-0629 (red bars) of Fe_3O_4 (a). XRD patterns of the OA-Fe_3O_4 NC/SiO_2/Si sample and an SiO_2/Si substrate (b).

Figure 2. Low-magnification cross-sectional TEM image (upper panel) and selected area electron diffraction pattern (lower panel) of OA-Fe_3O_4 NC self–assembled film.

Figure 3. High-resolution TEM image of a single grain (upper panel), nano beam diffraction pattern from the grain (lower left), and model of the diffraction pattern from an Fe_3O_4 crystal with the incident beam direction along the [110] axis (lower right).

Figure 4. *M-H* curves of the NCs and the sample (red line) at 200K (a). FC and ZFC *M-T* curves of the sample at H = 0.03 T (b). χ"-*T* curve for the ZFC sample with an f of 10 Hz (c).

Figure 5. *I-V* characteristics of the sample measured at 200K in H = 0, 0.5 and 1 T (a). dV/dI versus V plot of the *I-V* curves at 200K (b).

Figure 6. *I-V* characteristics of the sample measured at 295K in H = 0 and 0.2 T (a). dV/dI versus V plot of the *I-V* curves at 295K (b).

Figure 7. ln R_0 versus $T^{-1/2}$ plot for the sample with a line of best fit (a). Fowler-Nordheim plot of the *I-V* curves measured at 200K (b) and at 295K (c).

Figure 8. Fitting of the experimental *I-V* curves at 200K in H = 0 (upper panel) and 1 T (lower panel) to estimate the ξ value.

REFERENCES

[1] Yanase, A.: Siratori, K. *J. Phys. Soc. Jpn*. **1984,** *53*, 312-317.

[2] Zhang, Z.: Satpatahy, S. *Phys. Rev. B* **1991,** *44*, 13319-13331.

[3] Kohiki, S.: Okada, K.: Mitome, M.: Kohno, A.: Kinoshita, T.: Iyama, K.; Tsunawaki, F.: Deguchi, H. *ACS Appl. Mater. Interfaces* **2011,** *3*, 3589-3593.

[4] Inoue, J.: Maekawa, S. *Phys. Rev. B* **1996,** *53*, R11927-R11929.

[5] Julliere, M. *Phys. Lett.* **1975,** *54A*, 225-226.

[6] Poddar, P.: Fried, T.: Markovich, G. *Phys. Rev. B* **2002,** *65*, 172405.

[7] Zeng, H.: Black, C. T.: Sandstrom, R. L.: Rice, P. M.: Murray, C. B.: Sun, S. *Phys. Rev. B* **2006,** 73, 020402(R).

[8] Wang, W.: Yu, M.: Batzill, M.: He, J.: Diebold, U.: Tang, J. *Phys. Rev. B* **2006,** *73*, 134412.

[9] Wang, J.: Shi, J.: Tian, D.: Deng, H.: Li, Y.: Song, P.: Chen, C. *Appl. Phys. Lett*. **2007,** *90*, 213106.

[10] Kant, K. M.: Sethupathi, K.: Rao, M. S. R. *J. Appl. Phys.* **2008,** *103*, 07F318.

[11] Wang, W.: He, J.: Tang, J. *J. Appl. Phys.* **2009,** *105*, 07B105.

[12] Wang, S.: Yue, F. J.: Wu, D.: Zhang, F. M.: Zhong, W.: Du, Y. W. *Appl. Phys. Lett.* **2009,** *94*, 012507.

[13] Ziese, M.: Blythe, H. J. *J. Phys.: Condens. Matter* **2000**, *12*, 13-28.

[14] Taub, N.: Tsukernik, A.: Markovich, G. *J. Mag. Mag. Mater*. **2009,** *321*, 1933-1938.

[15] Murray, C. B.; Kagan, C. R.; Bawendi, M. G. *Ann. Rev. Mater. Sci*. **2000**, *30*, 545-610.

[16] Prasad, B. L. V.: Sorensen, C. M.: Klabunde, K. J. *Chem. Soc. Rev*. **2008**, *37*, 1871-1883.

[17] Tadmor, R.: Rosensweig, R. E.: Frey, J.: Klein, J. *Langmuir* **2000**,*16*, 9117-9120.

[18] Rybchenko, S. I.: Fujishiro, Y.: Takagi, Y.: Awano, M. *Phys. Rev. B* **2005**, *72*, 054424.

[19] Parthasarathy, R.; Lin, X. M.; Jaeger, H. M. *Phys. Rev. Lett*. **2001**, *87*, 186807.

[20] Middleton, A. A.; Wingreen, N. S. *Phys. Rev. Lett*. **1993**, *71*, 3198-3201.

[21] Kim, D.: Lee, N.: Park, M.: Kim, B. H.: An, K.: Hyeon, T. *J. Am. Chem. Soc*. **2009,** *131*, 454-455.

[22] Zhang, L.: Wu, J.: Liao, H.: Hou, Y.: Gao, S. *Chem. Commun.* **2009**, 4378-4380.

[23] Li, D.: Jiang, D.: Chen, M.: Xie, J.: Wu, Y.: Dang, S.: Zhang, J. *Mater. Lett.* **2010**, *64*, 2462-2464.

[24] Suzuki, M.: Fullem, S. I.: Suzuki, I. S.: Wang, L.: Zhong, C-J. *Phys. Rev. B* **2009,** *79*, 024418.

[25] Doman, J. L.: Fiorani, D.: Trone, E. *Adv. Chem. Phys.* **1997,** *98*, 283-494.

[26] Mydosh, J. A. *Spin Glasses: An Experimental Introduction*; Taylor & Frances: London, **1993**.

[27] Simmons, J. G. *J. Appl. Phys.* **1963,** *34*, 1793-1803.

[28] Tripathy, D.: Adeyeye, A. O.: Shannigrahi, S. *Phys. Rev. B* **2007,** *76*, 174429.

[29] Beebe, J. M.: Kim, B.: Gadzuk, J. W.: Frisbie, C. D.: Kushmerick, J. G. *Phys. Rev. Lett*. **2006**, *97*, 026801.

[30] Takahashi, S.: Maekawa, S. *Phys. Rev. Lett*. **1998**, *80*, 1758-1761.

[31] Zhang, X.-G.: Wen, Z. C.: Wei, H. X.: Han, X. F. *Phys. Rev. B* **2010**, *81*, 155122.

Figure 1 by S. K et al.

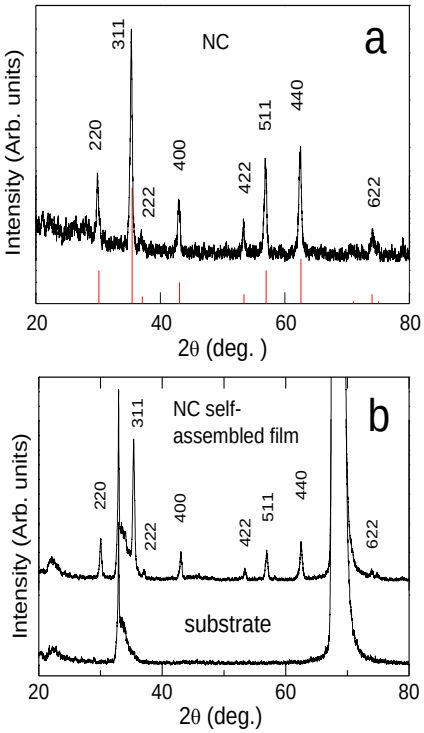

Figure 2 by S. K et al.

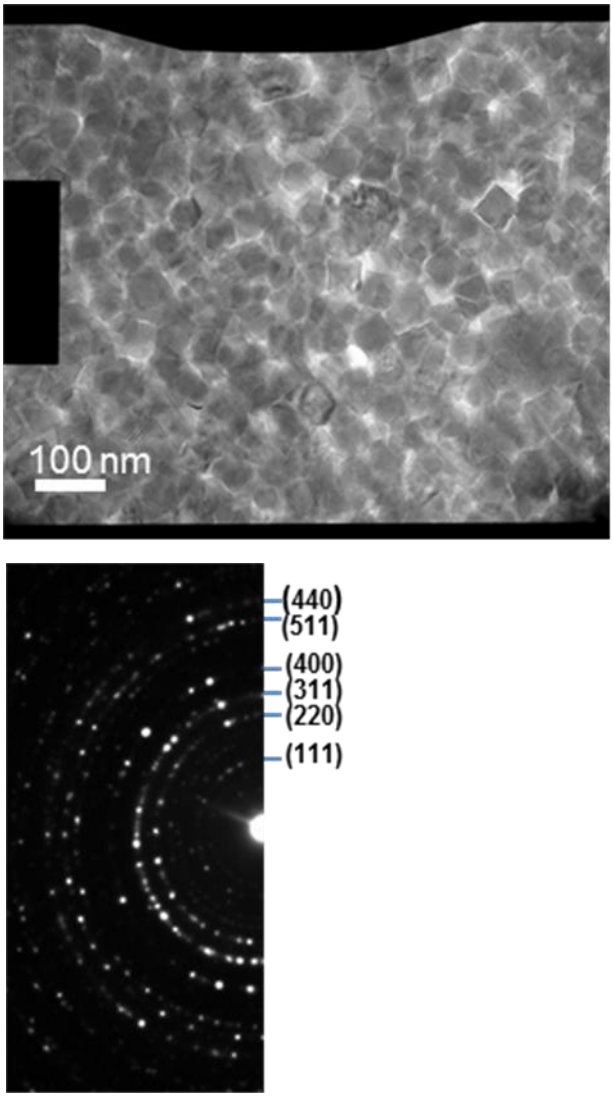

Figure 3 by S. K et al.

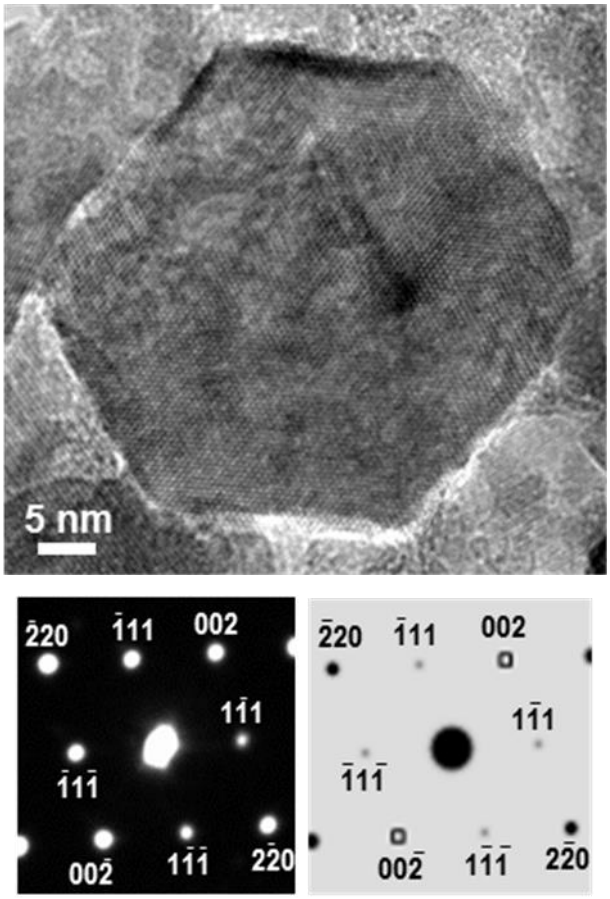

Figure 4 by S. K et al.

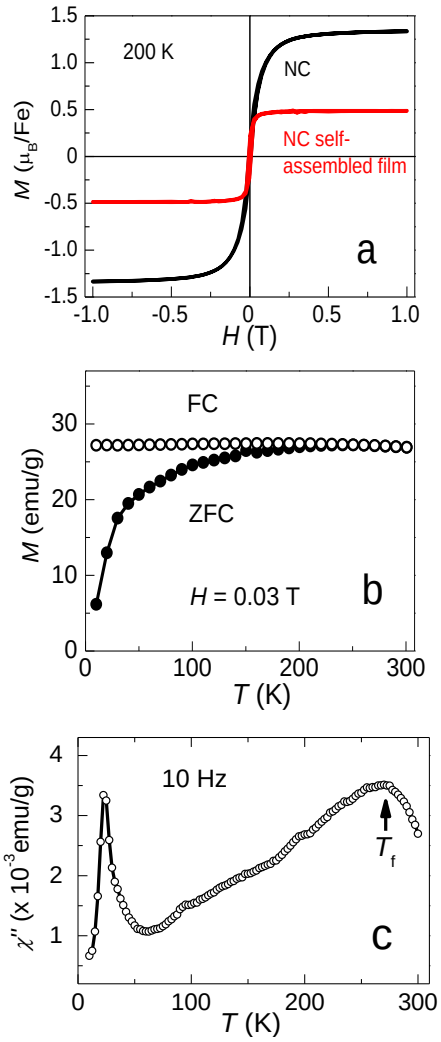

Figure 5 by S. K et al.

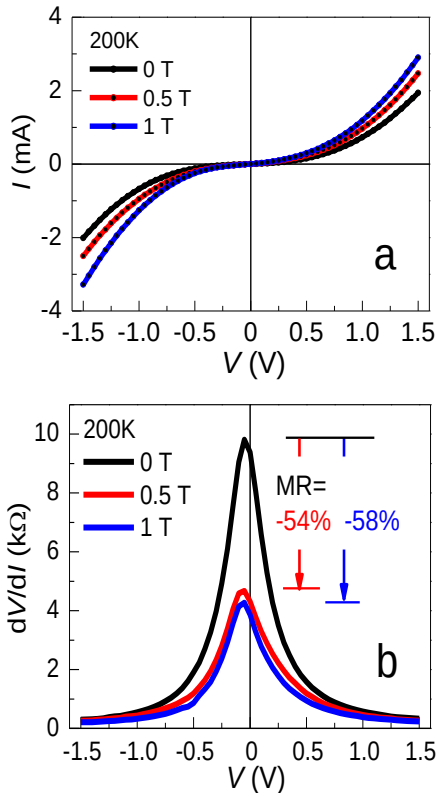

Figure 6 by S. K et al.

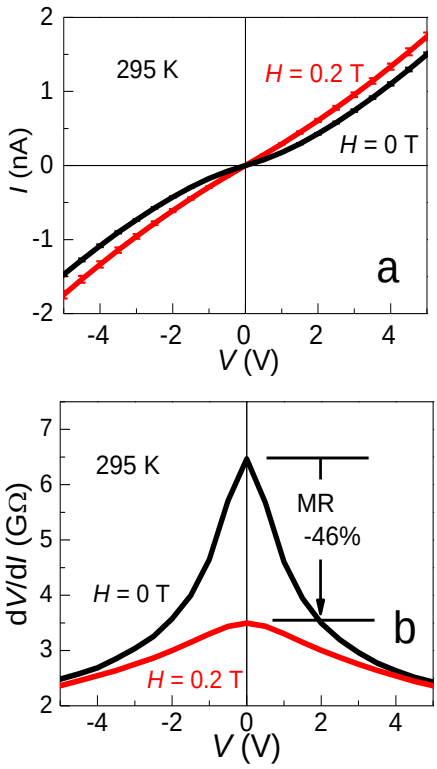

Figure 7 by S. K et al.

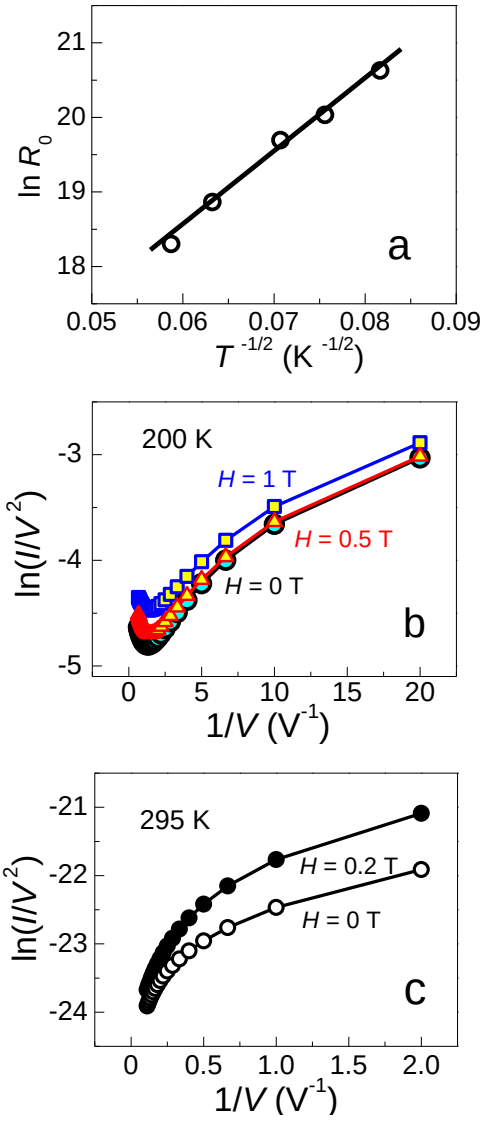

Figure 8 by S. K et al.